J|A|C|S
ARTICLES
Published on Web 12/02/2003

Structural Characterization of Crystalline Ternary Inclusion Compounds at the Air−Water Interface

David J. Plaut,[†] Stephen M. Martin,[†] Kristian Kjaer,[‡] Markus J. Weygand,[‡] Meir Lahav,[§] Leslie Leiserowitz,[§] Isabelle Weissbuch,*[,§] and Michael D. Ward*[,†]

Contribution from the Department of Chemical Engineering and Materials Science, University of Minnesota, Minneapolis, Minnesota 55455, Department of Materials and Interfaces, The Weizmann Institute of Science, 76100 Rehovot, Israel, and Materials Research Department, Risø National Laboratory, DK 4000 Roskilde, Denmark

Received July 8, 2003; E-mail: isabelle.weissbuch@weizmann.ac.il; wardx004@umn.edu

Abstract: Crystalline ternary inclusion monolayers consisting of a two-dimensional hydrogen-bonded host network of guanidinium (**G**) ions and organosulfonate (**S**) amphiphiles, and biphenylalkane guests, can be generated at the air−water interface through synergistic structural enforcement by hydrogen bonding and host−guest packing. Surface pressure−area isotherms of the 4′-hexadecylbiphenyl-4-sulfonate (C16BPS) amphiphile in the presence of **G**, with or without guest, are characterized by lift-off molecular areas expected for the **GS** sheet based on single-crystal X-ray structures of homologous bulk crystals. Intercalation of biphenylalkane guests (4-C_nH_{2n+1}−C_6H_4−C_6H_5, $n = 1$, 4, 6, 10, 16; denoted CnBP) between organosulfonate hydrophobes, which define pocketlike cavities in the **GS** monolayer host, afford ternary inclusion monolayers with a 1:1 host−guest stoichiometry. These inclusion monolayers are less compressible than the guest-free host, consistent with dense packing of the biphenylalkane moieties of the host and the biphenylalkane guests. The inclusion monolayers are distinguished from the amorphous guest-free host and from selected guanidinium-free mixed monolayers by structural characterization with grazing-angle incidence X-ray diffraction (GIXD). The GIXD data for the ternary (**G**)C16BPS:C16BP and (**G**)C16BPS:C6BP inclusion monolayers obtained upon compression are consistent with a rectangular unit cell. The dimensions of these unit cells and refinement of the GIXD data suggest a "rotated shifted ribbon" **GS** hydrogen-bonding motif similar to that observed in some bulk **GS** crystals, including (**G**)(ethylbiphenylsulfonate). GIXD reveals that (**G**)C16BPS:C16BP and (**G**)C16BPS:C6BP are more crystalline than the corresponding guanidinium-free mixed monolayers. The (**G**)C16BPS:C6BP inclusion monolayer is stable upon compression, even though the alkyl−alkyl host−guest interactions are reduced due to the shorter hexyl substituents of the guest, demonstrating an important reinforcing role for the hydrogen-bonded **GS** sheet. The structure of a C16BPS:tetracosane (C24) mixed monolayer is independent of **G**; the unit cell symmetry and dimensions suggest a structure governed by alkyl−alkane interactions that prohibit formation of a **GS** network. These results illustrate that the existence of ternary inclusion monolayers with an intact **GS** network requires guest molecules that are structurally homologous with the hydrophobes of the host, in this case biphenylalkanes. The observation of these inclusion compounds suggests an approach for introducing functional nonamphiphilic molecules to an air−water interface through inclusion in a well-defined host.

Introduction

Crystalline three-dimensional (3-D) organic frameworks have been examined extensively, owing to their ability to serve as hosts for inclusion of complementary guest molecules within well-defined cavities and potential applications in separations, catalysis, chemical and biological sensors, and electronic devices.[1] Host−guest complexes and inclusion compounds in *two-dimensional* molecular assemblies at the air−water interface are more limited in number than their 3-D counterparts, yet they span a range of architectures (Figure 1). Mixed monolayers, typically binary, formed at the air−water interface through specific interactions and stabilized by hydrophobe−hydrophobe contacts,[2,3] can be viewed as 2-D equivalents of bulk cocrystals (Figure 1a).[4] Amphiphiles that simply bind water-soluble guest molecules at or beneath the air−water interface through specific interactions, analogous to "coordinatoclathrate" host−guest complexes in 3-D crystals,[5] sometimes are characterized as

[†] University of Minnesota.
[‡] Risø National Laboratory.
[§] The Weizmann Institute of Science.

(1) (a) MacNicol, D. D.; McKendrick, J. J.; Wilson, D. R. In *Inclusion Compounds*; Atwood, J. L., Davies, J. E., MacNicol, D. D., Eds.; Academic Press: London, 1984; Vol. 2. (b) Simard, M.; Su, D.; Wuest, J. D. *J. Am. Chem. Soc.* **1991**, *113*, 4696. (c) Ermer, O.; Lindenberg, L. *Helv. Chim. Acta* **1991**, *74*, 825. (d) Endo, K.; Ezuhara, T.; Koyonagi, M.; Hideki, M.; Aoyama, Y.; *J. Am. Chem. Soc.* **1997**, *119*, 499.
(2) Kuzmenko, K.; Kjaer, K.; Als-Nielsen, J.; Lahav, M.; Leiserowitz, L. *J. Am. Chem. Soc.* **1999**, *121*, 2657.
(3) Gidalevitz, D.; Weissbuch, I.; Kjaer, K.; Als-Nielsen, J.; Leiserowitz, L. *J. Am. Chem. Soc.* **1994**, *116*, 3271.
(4) Burgi, H.-B.; Hulliger, J.; Langley, P. J. *Curr. Opin. Sol. State Mater. Sci.* **1998**, *3*, 425.

10.1021/ja0371404 CCC: $25.00

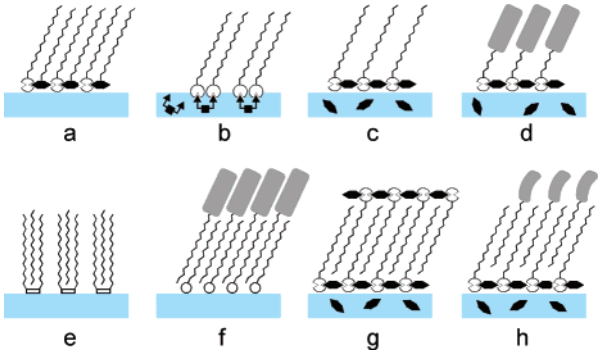

Figure 1. Schematic representations of various Langmuir monolayer architectures: (a) a mixed monolayer of amphiphiles assembled through specific interactions at the air−water interface; (b) a host monolayer of amphiphiles bound to solute guests below the air−water interface through specific interactions; (c) a host monolayer of amphiphiles bound to water-soluble "guest" molecules at the air−water interface through specific interactions (these guest molecules promote loose packing of the hydrophobes and amorphous character); (d) a crystalline host monolayer of amphiphiles, equipped with bulky terminal substituents, assembled through specific interactions with water-soluble guest molecules at the air−water interface; (e) a monolayer of cup-shaped amphiphiles with intercalated guest molecules above the air−water interface; (f) a crystalline mixed monolayer of amphiphiles assembled through nonspecific interactions, here displayed with bulky substituents on one of the amphiphiles; (g) a bilayer of self-interdigitated monolayers, each sufficiently spaced though specific binding with water-soluble spacer guest molecules; (h) a ternary monolayer composed of amphiphiles bound to solute molecules at the air−water interface through specific interactions, with nonamphiphilic guest molecules intercalating above the air−water interface.

host−guest complexes (Figure 1b−d).[6−11] Some of these have been proven to be crystalline by grazing incidence X-ray diffraction (GIXD).[12,13]

Conversely, host−guest assemblies that rely on nonspecific intercalation into cavities formed by amphiphile hydrophobes *above* the air−water interface are analogous to clathrates or coordination-assisted clathrates in 3-D crystals.[14] Fatty acid or alcohol amphiphiles can exhibit hostlike behavior, expanding to allow nonspecific intercalation to form crystalline mixed monolayers (Figure 1f).[15] Formation of a self-interdigitated crystalline bilayer has been achieved through the introduction of hydrophilic "spacer" molecules to the air−water interface, thereby separating the hydrophobes of the amphiphiles in one layer so that intercalation of the other is possible (Figure 1g).[16] Although such bilayers do not contain distinct host and guest components, the architecture of the bottom monolayer displays a key feature that is reminiscent of 3-D crystalline inclusion compounds—inherent cavities that permit inclusion of a structurally complementary component. These last two examples suggest that monolayers equipped with spacer molecules at the air−water interface can have inherent inclusion cavities between "preexpanded" hydrophobe arrays, affording hosts for *nonamphiphilic* guest molecules and generating two-dimensional inclusion compounds at the air−water interface (Figure 1h). In principle, this manner of guest intercalation could permit the introduction of functionality (i.e., the guest) at the air−water interface that otherwise may not be achievable.

One of our laboratories has reported numerous 3-D crystalline materials based on a highly persistent two-dimensional hydrogen-bonded network of guanidinium (**G**) ions, $C(NH_2)_3^+$, and sulfonate moieties (**S**) of organomonosulfonate and organodisulfonates.[17−20] The **GS** network, which typically adopts either a "quasihexagonal" or "shifted ribbon" motif, has been observed in more than 300 crystals derived from various organomonosulfonates and organodisulfonates, usually affording layered architectures. In the presence of suitable guest molecules, inclusion compounds can be generated with either (**G**)(organomonosulfonate) or $(\mathbf{G})_2$(organodisulfonate) hosts, wherein the organic substituents of the host support inclusion cavities between adjacent **GS** sheets.[21,22] The unusual persistence of the **GS** network has been attributed to the hydrogen-bonding complementarity of the **G** and **S** ions, the large number of hydrogen bonds within the network (up to six for each **G** and **S** ion), and an inherent structural flexibility of the **GS** sheet, which permits the host frameworks to achieve optimum packing with the guests, often resulting in packing that mimics that of the organic components alone.[23,24] The metrics of the **GS** sheet, in which the **S** sites are separated by 7.2−7.5 Å because of the intervening **G** ions, proscribes voids that permit interdigitation of organic groups from an opposing **GS** sheet, as observed in guest-free (**G**)(organomonosulfonates) that crystallize in the discrete bilayer architecture. This can be illustrated by the single-crystal X-ray structures of (**G**)(4′-methylbiphenyl-4-sulfonate) and (**G**)(4′-ethylbiphenyl-4-sulfonate). Even though these two compounds display different hydrogen-bonded motifs (quasihexagonal and shifted ribbon, respectively), both exhibit the bilayer architecture with interdigitation of organic groups (Figure 2).[25,26]

These features suggested that **GS** monolayers based on 4′-alkylbiphenyl-4-sulfonates could serve as two-dimensional hosts at the air−water interface, with inclusion cavities for intercalat-

(5) Weber, E. In *Topics in Current Chemistry*; Springer-Verlag: Berlin, 1987; Vol. 140.
(6) Bohanon, T. M.; Denziger, S.; Fink, R.; Paulus, W.; Ringsdorf, H.; Weck, M. *Angew. Chem., Int. Ed. Engl*. **1995**, *34*, 58.
(7) (a) Ariga, K.; Kunitake, T. *Acc. Chem. Res*. **1998**, *31*, 371. (b) Cha, X.; Ariga, K.; Kunitake, T. *J. Am. Chem. Soc.* **1996**, *118*, 9545. (c) Sasaki, D. Y.; Kurihara, K.; Kunitake, T. *J. Am. Chem. Soc.* **1992**, *114*, 10994.
(8) Siegel, S.; Kindermann, M.; Regenbrecht, M.;. Vollhardt, D.; von Kiedrowski, G. *Prog. Colloid Polym. Sci*. **2000**, *115*, 233.
(9) Plaut, D. J.; Lund, K. M.; Ward, M. D. *Chem. Commun*. **2000**, *9*, 769.
(10) Tyson, J. C.; Moore, J. L.; Hughes, K. D.; Collard, D. M. *Langmuir* **1997**, *13*, 2068.
(11) Kuzmenko, I.; Kindermann, M.; Kjaer, K.; Howes, P. B.; Als−Nielsen, J.; Granek, R.; von Kiedrowski, G.; Leiserowitz, L.; Lahav, M. *J. Am. Chem. Soc.* **2001**, *123*, 3771.
(12) Kuzmenko, I.; Rapaport, H.; Kjaer, K.; Als-Nielsen, J.; Weissbuch, I.; Lahav, M.; Leiserowitz, L. *Chem. Rev*. **2001**, *101*, 1659.
(13) Alonso, C.; Eliash, R.; Jensen, T. R.; Kjaer, K.; Lahav, M.; Leiserowitz, L. *J. Am. Chem. Soc.* **2001**, *123*, 10105.
(14) Ashwell, G. J.; Dyer, A. N.; Green, A.; Sato, N.; Sakuma, T. *J. Mater. Chem*. **2000**, *10*, 2473.
(15) Alonso, C.; Kuzmenko, I.; Jensen, T. R.; Kjaer, K.; Lahav, M.; Leiserowitz, L. *J. Phys. Chem. B* **2001**, *105*, 8563.
(16) Kuzmenko, I.; Buller, R.; Bouman, W. G.; Kjaer, K.; Als-Nielsen, J.; Lahav, M.; Leiserovitz, L. *Science* **1996**, *274*, 2046.
(17) Russell, V. A.; Etter, M. C.; Ward, M. D. *J. Am. Chem. Soc.* **1994**, *116*, 1941.
(18) Swift, J. A.; Pivovar, A. M.; Reynolds, A. M. *J. Am. Chem. Soc*. **1998**, *24*, 5887.
(19) Evans, C. C.; Sukarto, L.; Ward, M. D. *J. Am. Chem. Soc*. **1999**, *121*, 320.
(20) Holman, K. T.; Pivovar, A. M.; Ward, M. D. *Science* **2001,** *294*, 1907
(21) Russell, V. A.; Evans, C. C.; Li, W.; Ward, M. D. *Science* **1997**, *276*, 575.
(22) Holman, K. T.; Pivovar, A. M.; Swift, J. A.; Ward, M. D. *Acc. Chem. Res*. **2001**, *34*, 107.
(23) Holman, K. T.; Ward, M. D. *Angew. Chem., Int. Ed*. **2000**, *39*, 1653.
(24) Holman, K. T.; Martin, S. M.; Parker, D. P.; Ward, M. D. *J. Am. Chem. Soc*. **2002**, *123*, 4421.
(25) Single-crystal X-ray structure data for (**G**)(4′-methylbiphenyl-4-sulfonate) (**1**): formula $C_{14}H_{17}N_3O_3S$; formula weight 307.37; crystal system monoclinic; space group $P2_1/n$; a = 11.902(3) Å; b = 7.561(7) Å; c = 34.130(7) Å; β = 94.679(5)°; V = 3061.4(1) Å^3, temperature 173(2) K; Z = 8; R1($I > 2\sigma(I)$) = 0.0580; wR2($I > 2\sigma(I)$) = 0.1899; GOF = 1.096.
(26) Single-crystal X-ray structure data for (**G**)(4′-ethylbiphenyl-4-sulfonate) (**2**): formula $C_{15}H_{19}N_3O_3S$; formula weight 321.40; crystal system monoclinic; space group $P2_1$; a = 12.180(4) Å; b = 7.250(2) Å; c = 17.807(5) Å; β = 100.204(6)°; V = 1547.5(8) Å^3, temperature 173(2) K; Z = 4; R1($I > 2\sigma(I)$) = 0.0594; wR2($I > 2\sigma(I)$) = 0.1420; GOF = 1.032.

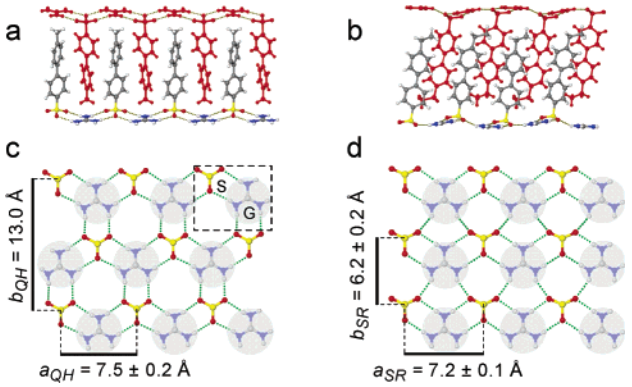

Figure 2. Interdigitated bilayer structures adopted in bulk 3-D crystals of (a) (**G**)(4′-methylbiphenyl-4-sulfonate) and (b) (**G**)(4′-ethylbiphenyl-4-sulfonate), as determined by single-crystal X-ray diffraction. Half of the bilayer is depicted in red to aid visualization of the interdigitation. Top view of the (c) quasi-hexagonal and (d) shifted ribbon **GS** hydrogen-bonded network observed in crystalline **GS** compounds, including the structures in (a) and (b), respectively. The gray circles represent the regions that may be occupied by guest molecules in inclusion monolayers. The areas per formula unit are 48.8 Å^2 (box in (c)) and 44.6 Å^2 (d).

Chart 1

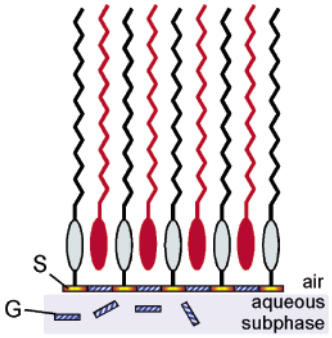

ing homologous guest molecules. The molecular area of a **GS** unit, on the basis of single-crystal structures of compounds with flat hydrogen-bonded **GS** sheets, is 48 Å^2. Assuming a cross-sectional area of 21 Å^2 for an alkyl chain and 23 Å^2 for a phenyl ring, the cross-sectional area of an inclusion cavity in a **GS** monolayer with biphenylalkane substituents would be roughly 25 Å^2, sufficient for intercalation of an aliphatic or aromatic guest molecule (Chart 1).

Herein we report the formation and characterization, principally with GIXD, of ternary inclusion monolayers that result from intercalation of guest molecules into a two-dimensional hydrogen-bonded host network of guanidinium ions and organomonosulfonate amphiphiles. These inclusion monolayers, consisting of **G**, 4′-hexadecylbiphenyl-4-sulfonate (C16BPS), and various biphenylalkanes **1**−**5** (Chart 2), possess certain structural features observed in their 3-D crystalline counterparts. Surface pressure−area isotherms and GIXD data combined revealed a structure-enforcing role for the **GS** network, which stabilized the inclusion monolayers toward collapse and loss of guest molecules. In contrast, guests **6** and **7** formed host−guest monolayers with structures that precluded formation of an ordered **GS** network in a manner that suggested an important role for interactions between host and guest biphenyl groups. These results illustrate that the existence of ternary inclusion monolayers, with the **GS** network intact, requires guest molecules that are structurally homologous with the hydrophobes of the host, in this case biphenylalkanes. The observation of

Chart 2

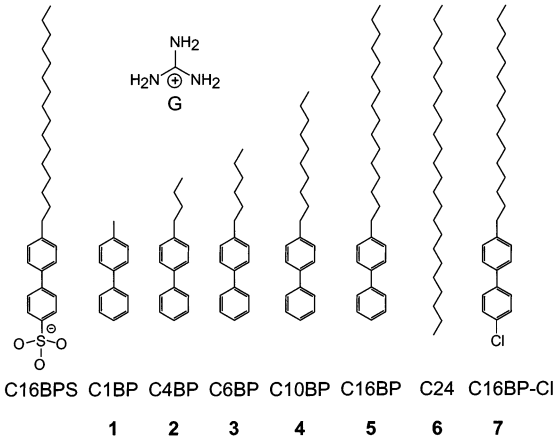

these inclusion compounds suggests an approach for introducing functional nonamphiphilic molecules to an air−water interface through inclusion in a well-defined host.

Results and Discussion

Guest-Free Monolayers. The surface pressure−area (π−A) isotherm of a C16BPS monolayer on pure water revealed the formation of a condensed phase with an extrapolated molecular area of A_{mol} = 28 Å^2/sulfonate (from the rising portion of the isotherm in Figure 3a). This value is larger than that expected for close-packed alkyl chains (ca. 19−21 Å^2)[27] or biphenyl molecules (ca. 23 Å^2),[28] revealing the influence of the sulfonate headgroup. Isotherms of the same amphiphile on an aqueous subphase of $\mathbf{G}_2CO_3$, however, exhibited features distinct from isotherms over pure water. Specifically, when **G** was present in the subphase, the surface pressure exhibited a discernible increase at larger molecular areas (this area is referred to herein as $A_{lift-off}$) and the isotherm rose less steeply. The lift-off area increased logarithmically with increasing **G** concentration in the range $0.0001 < [\mathbf{G}] < 0.01$ M, eventually achieving a limiting value of $A_{lift-off}$ = 52 Å^2/sulfonate beyond this concentration range (Figure 4). This area agrees with that expected, based on 3-D single-crystal structures, for either of the planar **GS** networks in Figure 2, signaling a 1:1 hydrogen-bonded **GS** monolayer for $[\mathbf{G}] > 0.01$ M. The collapse pressure of the hydrogen-bonded monolayer was lower than in the absence of **G**, possibly reflecting the coexistence of crystalline and amorphous phases just prior to collapse. A specific hydrogen-bonding role of the **G** ion in the expansion of the C16BPS monolayer was substantiated by isotherms collected over aqueous 0.01 M Na_2CO_3 or 0.1 M KCl, which produced extrapolated molecular areas of A_{mol} = 28 Å^2/sulfonate, identical with the value for water alone. Furthermore, C16BPS amphiphile spread over a subphase of aqueous 0.02 M $\mathbf{G}^+Cl^-$ exhibited an isotherm with identical shape and lift-off area as the isotherm collected over a subphase containing 0.01 M $\mathbf{G}_2CO_3$ (equivalent guanidinium concentrations).

GIXD scattering patterns for C16BPS on pure water (Figure 3b), measured at selected points along the π−A isotherm in the range $25 < A_{mol} < 50$ Å^2/sulfonate, exhibited two Bragg peaks

(27) Gerson, A. R.; Roberts, K. J.; Sherwood, J. N. *Acta Crystallogr.* **1991**, *B47*, 280.
(28) Charbonneau, G. P.; Delugeard, Y. *Acta Crystallogr.* **1977**, *B33*, 1586.

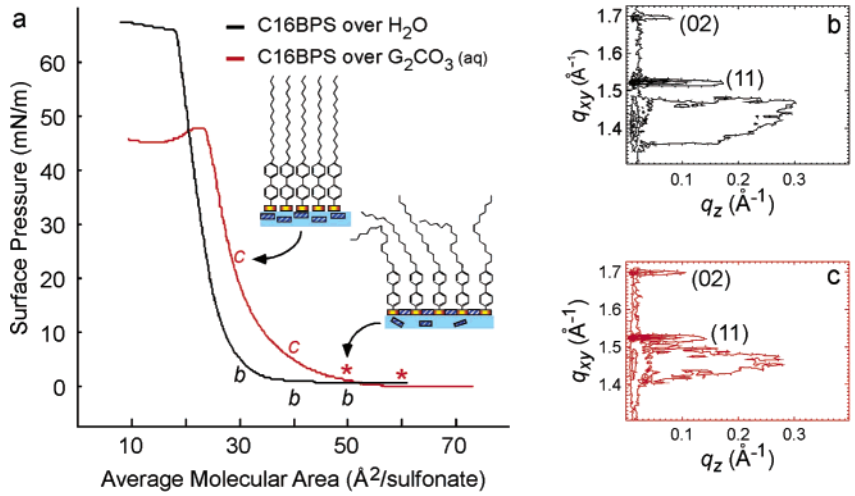

Figure 3. (a) $\pi-A$ isotherms of C16BPS on pure water (black) and C16BPS on 0.01 M $\mathbf{G}_2CO_3$ (red). GIXD patterns shown as two-dimensional contour plots of the scattered intensity, $I(q_{xy},q_z)$, measured for (b) C16BPS on pure water at $A_{mol} = 30$ Å^2/sulfonate (the GIXD pattern was essentially unchanged within the range 25 Å^2 < A_{mol} < 50 Å^2/sulfonate) and (c) C16BPS on 0.01 M $\mathbf{G}_2CO_3$ at $A_{mol} = 30$ Å^2/sulfonate (a similar signal resulted throughout the range A_{mol} < 42 Å^2/sulfonate). The schematics of the monolayers depict an amorphous (no diffraction observed) (**G**)C16BPS monolayer at low pressures (denoted on the isotherm by the red asterisks) and a crystalline C16BPS monolayer at higher pressures, where the **G** ion is forced out of the air−water interface so close packing of the chains can be achieved.

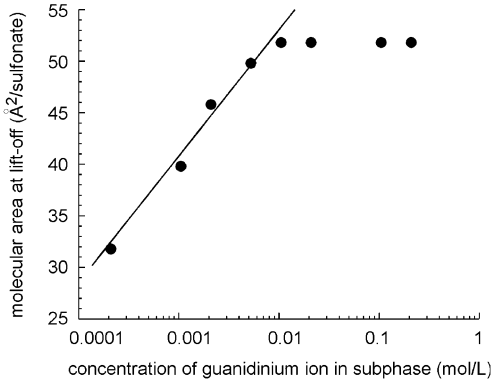

Figure 4. Dependence of the lift-off area on the **G** subphase concentration for a C16BPS monolayer. The liftoff area achieves a plateau of 52 Å^2/molecule at [**G**] > 0.01 M, consistent with the area of a **GS** network. The line shown is the logarithmic fit of the first five data points, with a correlation factor $R = 0.99$.

at $q_{xy} = 1.52$ and 1.70 Å^{-1}. These two peaks can be indexed to a pseudo-centered rectangular unit cell containing two molecules and having lattice parameters $a = 4.99$ Å, $b = 7.39$ Å, and $A_{cell} = 36.8$ Å^2. This unit cell resembles those for typical monolayers of aliphatic surfactants with alkyl chains aligned perpendicular to the air−water interface.[29] Analysis of the full width at half-maximum (fwhm) of the Bragg peaks (q_{xy}) and Bragg rods (q_z) indicated an average domain coherence length of ca. 900 Å and a monolayer thickness of ca. 35 Å, respectively. A weak Bragg peak also was observed at $q_{xy} = 1.40$ Å^{-1}, but the fwhm of this peak corresponded to a coherence length (ca. 45 Å) that was substantially smaller than the domains of the rectangular cell, revealing that this peak was due to a second phase with lower crystallinity. The observation of a single Bragg peak suggests a hexagonal cell ($a = 5.16$ Å), with a thickness of ca. 14 Å, as deduced from the fwhm value of its Bragg rod.

At A_{mol} < 42 Å^2/sulfonate a C16BPS monolayer over 0.01 M $\mathbf{G}_2CO_3$ produced a diffraction pattern (Figure 3c) similar to that obtained over pure water (Figure 3b). At A_{mol} > 42 Å^2/sulfonate, however, no diffraction pattern was observed. This is not surprising; formation of the **GS** network at the air−water interface, which is supported by the lift-off area of $A_{lift-off} =$ 52 Å^2/sulfonate, would preclude close packing of the C16BPS hydrophobes to the extent that these scattering centers would be disordered. Compression of the film would expel the **G** ions from the **GS** network into the subphase, thereby allowing formation of the guanidinium-free C16BPS monolayer.

Crystalline Monolayers with Biphenylalkane Intercalates. A low-density monolayer like (**G**)C16BPS offers the prospect for intercalation of nonamphiphilic guest molecules within the cavities generated by the hydrophobes of the host framework. The $\pi-A$ isotherm for a 1:1 solution of C16BPS and 4-hexadecylbiphenyl (C16BP) guest spread over 0.01 M $\mathbf{G}_2CO_3$ revealed $A_{lift-off} = 52$ Å^2/sulfonate (Figure 5a), identical with the behavior in the absence of C16BP. Grazing angle FT-IR of a Langmuir−Blodgett (LB) monolayer on a gold-coated glass substrate, prepared by transfer at a surface pressure of 10 mN/m, revealed N−H bending modes at 1550−1750 cm^{-1}. These modes also were observed in bulk crystals of guanidinium alkylbiphenylsulfonates, substantiating the existence of a hydrogen-bonded **GS** network. Further characterization based on N−H stretching modes between 3100 and 3500 cm^{-1} was prohibited by the presence of persistent water, probably bound to the film through hydrogen bonding. Unlike its guest-free counterpart, the isotherm of this (**G**)C16BPS:C16BP monolayer was very steep, signifying an increase in monolayer rigidity owing to inclusion of C16BP. Notably, the $\pi-A$ isotherm for a 1:1 mixture of C16BPS and C16BP on a pure water subphase was somewhat similar, differing only with respect to the collapse pressure. In the absence of other evidence, one would surmise that the two isotherms in Figure 5 are associated with the identical monolayers. GIXD measurements, however, revealed that the monolayers over pure water and over 0.01 M $\mathbf{G}_2CO_3$ *adopt different packing arrangements*. Furthermore, both structures differ from that of the crystalline phase observed in the absence of the guest, as evidenced from comparison of the diffraction patterns in Figures 3 and 5.

(29) Kuzmenko, I.; Kaganer, V. M.; Leiserowitz, L. *Langmuir* **1998**, *14*, 3882.

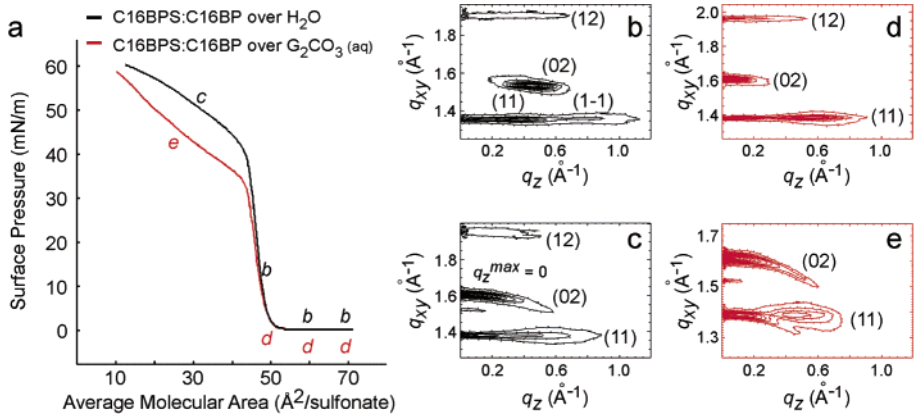

Figure 5. (a) $\pi-$A isotherms of C16BPS:C16BP on pure water (black) and 0.01 M $\mathbf{G}_2CO_3$ (red). GIXD contour plots of the scattered intensity measured from C16BPS:C16BP on (b) pure water at 48 < A_{mol} < 70 Å^2/sulfonate, (c) pure water at A_{mol} < 38 Å^2/sulfonate, (d) 0.01 M G_2CO_3 at 48 < A_{mol} < 70 Å^2/sulfonate, and (e) 0.01 M G_2CO_3 at A_{mol} < 25 Å^2/sulfonate.

Table 1. Structural Parameters of Uncompressed Crystalline C16BPS-Based Monolayers on Water and 0.01 M G_2CO_3[a]

	water only						0.01 M $\mathbf{G}_2CO_3$					
guest	a (Å)	b (Å)	γ (deg)	A_{cell} (Å^2)	t (deg)[b]	ψ[c]	a (Å)	b (Å)	γ (deg)	A_{cell} (Å^2)	t (deg)[b]	ψ (deg)[c]
none	4.99	7.39	90	36.8	0	0						
C16BP	5.58	8.13	89.8	45.4	31	151	5.58	7.83	90	43.7	26	0
C6BP	5.48	8.26	90	45.3	8	0	5.51	8.15	90	44.9	8	0
C16BP−Cl[d]	5.68	8.32	90	47.3	35	149	5.56	8.11	90	45.1	31	151
					30	139						
C24	4.99	9.04	90	45.1	29	90	4.99	9.04	90	45.1	29	90

[a] Structural parameters determined from GIXD data acquired at a surface pressure of 0 mN/m. [b] t = tilt angle of the alkyl chains from the normal to the air−water interface (see Figure 6). [c] ψ = azimuthal direction with respect to the a axis along which tilt, t, occurs (see Figure 6). [d] On water only, two phases with identical unit cell parameters but slightly different t and ψ values were apparent in the Bragg rod. The two contributions were separated by least-square fittings. See the Supporting Information.

GIXD (Figure 5b) of the C16BPS:C16BP mixed monolayer on pure water, measured at surface pressures less than 5 mN/m where A_{mol} > 48 Å^2/sulfonate, produced Bragg peaks (q_{xy}) that could be indexed to a near-rectangular unit cell, containing two molecules, with lattice parameters a = 5.58 Å, b = 8.13 Å, γ = 89.8°, and A_{cell} = 45.4 Å^2 (Table 1). On the basis of the q_z position of the intensity maxima along the Bragg rods, $I(q_z)$, the alkyl chains tilt 31° from the normal to the air−water interface at an azimuthal direction 151° from the a axis. The measured fwhm of the Bragg peaks corresponds to a coherence length of 190 Å. The monolayer packing arrangement was refined on the basis of X-ray structure factor calculations using an atomic coordinate model of a unit cell based on known 3-D crystal structures. Using the SHELX97 program adapted for 2-D crystals, the packing arrangement for a unit cell containing one C16BPS amphiphile and one C16BP guest was refined with each molecule constrained separately as a rigid body. The best refinement was achieved with the alkyl chain of C16BPS and C16BP having C1−C2−C3−C4 and C3−C4−C5−C6 dihedral angles locked to angles measuring 155° (C1 being the carbon atom attached to the biphenyl), with the remaining portion of the chains being all-trans (Figure 6). This results in a substantial tilt of the biphenyl rings from the surface normal. Upon compression of the C16BPS:C16BP mixed monolayer to A_{mol} = 38 Å^2/sulfonate the {02} Bragg rod became skewed (Figure 5c), which signifies buckling of the monolayer.[30,31] Furthermore, the maximum position of intensity became $q_z^{max} = 0$ Å^{-1} for all Bragg rods, indicating a transformation to a new phase in which the alkyl chains were perpendicular to the air−water interface. The diffraction data for this more compressed monolayer were indexed to a unit cell of a = 5.6 Å, b = 7.8 Å, γ = 90°, and A_{cell} = 43.7 Å^2 and the domain coherence length was unchanged.

The GIXD contour plots for the(**G**)C16BPS:C16BP monolayer (Figure 5d), collected over 0.01 M $\mathbf{G}_2CO_3$ at A_{mol} > 48 Å^2/sulfonate, clearly revealed a crystal structure different from the monolayer in the absence of **G**, *verifying the existence of a ternary inclusion compound at the air−water interface*. The data support a rectangular cell with two molecules and lattice dimensions a = 5.58 Å, b = 7.83 Å, and A_{cell} = 43.7 Å^2. The alkyl chains tilt along the a axis by 26° from the normal to the air−water interface, as deduced from the q_z position of the intensity maximum along the (11) Bragg rod. The measured fwhm of the Bragg peaks corresponds to a coherence length of 380 Å, a factor of 2 larger than that measured for the C16BPS:C16BP monolayer without **G** in the subphase. Similar to the C16BPS:C16BP monolayer, the GIXD pattern of the compressed (**G**)C16BPS:C16BP monolayer at A_{mol} < 25 Å^2/sulfonate (Figure 5e) displayed a skewing of the Bragg rods associated with a buckling of a stiff monolayer.

Using the rectangular shifted ribbon hydrogen-bonding motif of guanidinium 4′-ethylbiphenyl-4-sulfonate (**G**C2BPS) as a

(30) Kjaer, K.; Bouwman, W. G. X-ray 2D-Powder Diffraction Methods for Films at Liquid Surfaces. In *Annual Progress Report of the Department of Solid State Physics 1 January−31 December 1994*; Lindgård, P.-A., Bechgaard, K., Clausen, K. N., Feidenhans'l, R., Johannsen, I., Eds.; RISØ-R-779(EN); Risø National Laboratory; Roskilde, Denmark; Jan 1995; p 79.

(31) Howes, P. B., Kjaer, K. X-ray Diffraction from Curved Thin Films. *Annual Progress Report of the Department of Solid State Physics 1 January−31 December 1996*; Jørgensen, M., Bechgaard, K., Clausen, K. N., Feidenhans'l, R., Johannsen, I., Eds.; RISØ-R-933(EN); Risø National Laboratory; Roskilde, Denmark; Jan 1997; p 71.

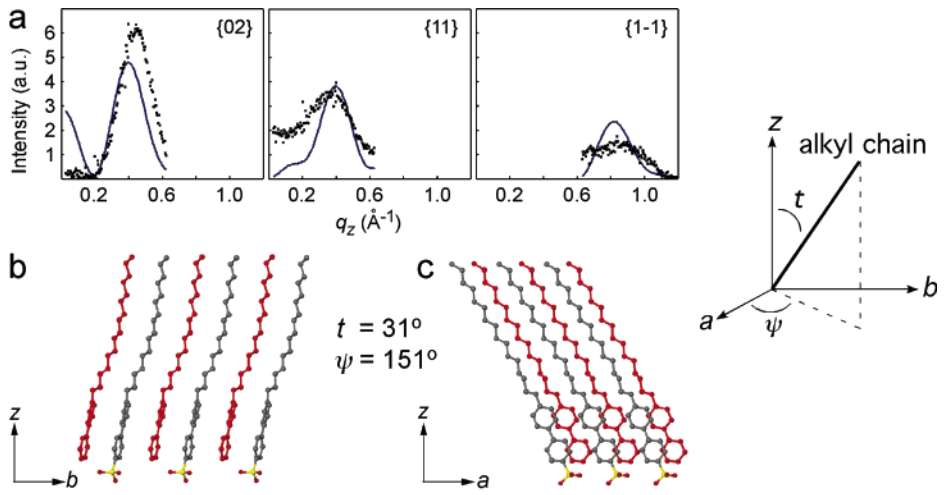

Figure 6. (a) Experimental (black dots) and calculated (blue lines) Bragg rod intensity profiles, $I(q_z)$, for C16BPS:C16BP over pure water. Refined packing arrangements of the C16BPS:C16BP monolayer viewed down the (b) *a* and (c) *b* axes. C16BP molecules are depicted in red. The tilt angle, *t*, and the azimuthal angle, ψ, of the alkyl chains are defined according to the panel at the right.

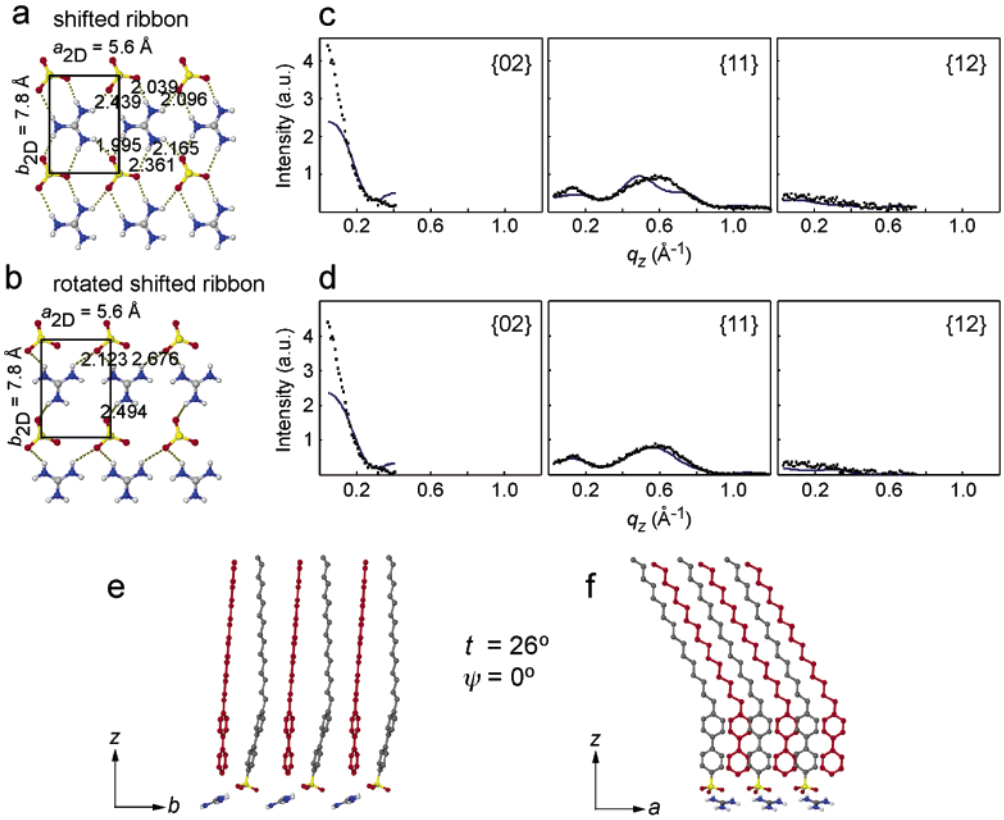

Figure 7. Rectangular (a) shifted ribbon and (b) rotated shifted ribbon **GS** hydrogen-bonded motifs used in the refinement of the (**G**)C16BPS:C16BP monolayer. The hexadecylbiphenyl groups are omitted for clarity, and the N−H···O−S hydrogen bond distances are denoted (in Å). Experimental (black dots) and calculated (blue lines) Bragg rod intensity profiles, $I(q_z)$, for (**G**)C16BPS:C16BP with (c) the shifted ribbon motif and (d) the rotated shifted-ribbon motif. The refinement of the {11} Bragg rod is improved in (d). Panels (e) and (f) depict the refined packing arrangements of the (**G**)C16BPS:C16BP monolayer with a "rotated shifted ribbon" motif, as viewed down the (e) *a* and (f) *b* axes. C16BP guests are depicted in red. The angles *t* and ψ are defined in Figure 6.

guide (Figure 2, above), an atomic coordinate model of the (**G**)C16BPS:C16BP monolayer packing arrangement was constructed and refined with the GIXD data. The refinement was performed with an asymmetric unit consisting of a guanidinium−sulfonate amphiphile ion pair and a C16BP guest molecule, each constrained as separate rigid bodies. Refinements based on a shifted ribbon **GS** motif like that observed in bulk crystals, but with the hydrogen-bonding distances adjusted to compensate for the different unit cell dimensions (smaller *a* and larger *b*), produced acceptable fits (Figure 7c). An alternative motif with the **G** and **S** ions rotated so that some hydrogen bonds are unfulfilled (Figure 7d), however, improved the fit to the {11} Bragg rod. Although this variant of the shifted ribbon motif has not been observed in bulk crystals, water from the subphase may perturb the typical **GS** motifs through hydrogen bonding with the **G** and **S** ions at the air−water interface, possibly becoming part of the hydrogen-bonded network. The structure was refined with all-trans alkyl chains for both the host and the

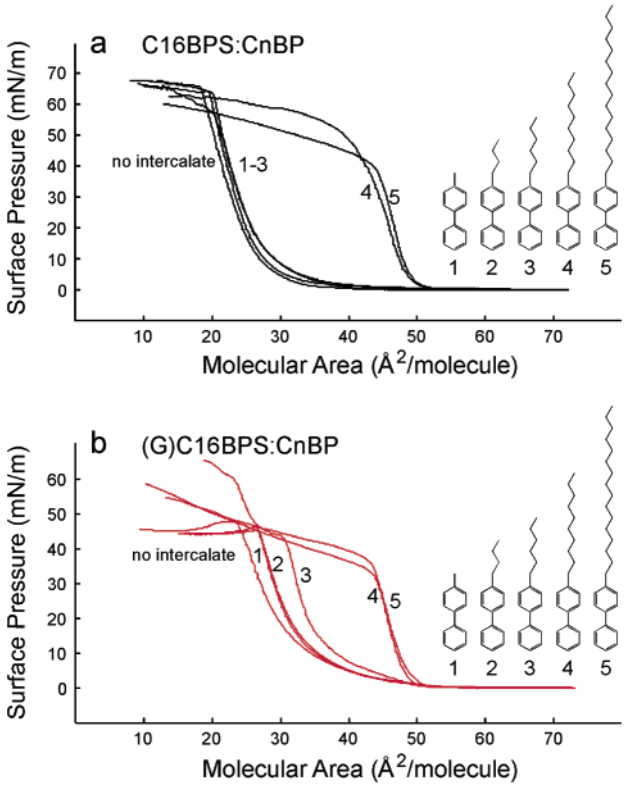

Figure 8. $\pi-A$ isotherms of (a) C16BPS:CnBP on pure water and (b) C16BPS:CnBP on 0.01 M $\mathbf{G}_2CO_3$ with guest molecules C1BP (1), C4BP (2), C6BP (3), C10BP (4), and C16BP (5).

guest, with pseudo-herringbone[29] alkyl−alkyl and biphenyl−biphenyl host−guest motifs (Figure 7e,f).

To probe the contribution of host−guest interactions above the air−water interface to the stability of these ternary inclusion monolayers, the biphenylalkane guests 4-$C_nH_{2n+1}-C_6H_4-C_6H_5$, where $n = 1$, 4, 6 and 10, denoted CnBP, were examined (Chart 2). The isotherm of the C16BPS:C10BP monolayer (no **G** present) resembles that of the C16BPS:C16BP monolayer with $A_{lift-off} = 52$ Å^2/sulfonate and a steep increase of surface pressure upon compression (Figure 8a). In contrast, the isotherms of the C16BPS:C1BP, C16BPS:C4BP, and C16BPS:C6BP mixed monolayers are essentially identical with the isotherm of the C16BPS monolayer *without* guest intercalate, with similar slopes upon compression and nearly identical molecular areas at collapse (ca. 20 Å^2/sulfonate). The isotherms therefore signify robust 1:1 mixed monolayers for guests **4** and **5**, which have long alkyl tails, but substantially less stability for guests **1**−**3**.

The $\pi-A$ isotherms for the (**G**)C16BPS:CnBP monolayers (Figure 8b) parallel those observed in the absence of **G**, albeit with some noticeable differences. The collapse pressures are generally lower. Furthermore, the (**G**)C16BPS:CnBP monolayers with guests **1**−**3** exhibit a perceptible $A_{lift-off}$ at ca. 50 Å^2/sulfonate and have larger extrapolated limiting areas, features that are consistent with the **GS** sheet and host−guest inclusion at low surface pressures. The slopes of the isotherms increase in the order **1** < **2** < **3** < **4** < **5**, reflecting increasing monolayer stiffness due to increasing alkyl chain length and packing density. The isotherms in Figure 8b, particularly those for guests **1**−**3**, indicate that **GS** hydrogen bonding and host−guest

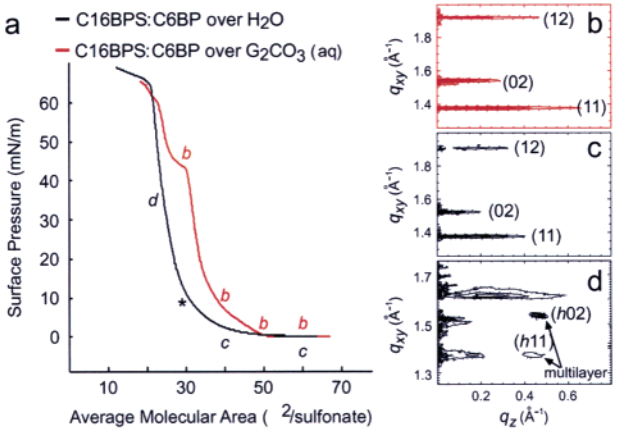

Figure 9. (a) $\pi-A$ isotherms of C16BPS:C6BP on pure water (black) and on 0.01 M $\mathbf{G}_2CO_3$ (red). GIXD contour plots of the scattered intensity measured from C16BPS:C6BP on (b) 0.01 M $\mathbf{G}_2CO_3$ from 30 < A_{mol} < 70 Å^2/sulfonate, (c) pure water at 60 and 40 Å^2/sulfonate, and (d) pure water at 22.5 Å^2/sulfonate. The diffraction pattern observed at the molecular area corresponding to the asterisk is illustrated in Figure 11 as a 1-D Bragg peak representation.

interactions both contribute to stability and properties of the inclusion monolayers.

The influence of guest alkyl chain length on monolayer structure and stability was probed in detail for a selected member of the biphenylalkane series, C6BP (**3**). The GIXD patterns measured from (**G**)C16BPS:C6BP (Figure 9b) on 0.01 M $\mathbf{G}_2CO_3$ consisted of Bragg peaks that could be indexed to a rectangular unit cell of $a = 5.51$ Å, $b = 8.15$ Å, and $A_{cell} = 44.9$ Å^2. The alkyl chains tilt along the a axis by 8° from the normal to the air−water interface, as calculated from the q_z position of the intensity maxima along the Bragg rods. The measured fwhm of the Bragg peaks corresponded to a coherence length >1200 Å. The structure of the (**G**)C16BPS:C6BP monolayer was deduced by refinement of an atomic coordinate model in a unit cell containing the (**G**)C16BPS ion pair and the C6BP guest molecule, each constrained as separate rigid bodies. The best refinement produced a structure with the rotated shifted ribbon **GS** hydrogen-bond motif and a pseudo-herringbone arrangement between the biphenyl moieties and alkyl chains of the host and guest (Figure 10). Notably, the GIXD pattern associated with the (**G**)C16BPS:C6BP inclusion monolayer did not change when compressed to areas in the range 30 < A_{mol} < 60 Å^2/sulfonate.

At A_{mol} > 40 Å^2/sulfonate, a C16BPS:C6BP mixed monolayer on pure water produced a GIXD pattern (Figure 9c) similar to that observed for (**G**)C16BPS:C6BP, suggesting similar host−guest packing in the two monolayers. The integrated intensities of all the Bragg peaks, however, are 5 times smaller for C16BPS:C6BP, and the fwhm values of the Bragg peaks correspond to a smaller coherence length (700 Å). Both features signify reduced crystallinity for the C16BPS:C6BP monolayer. Furthermore, unlike (**G**)C16BPS:C6BP, the GIXD pattern of C16BPS:C6BP changed substantially upon compression (Figure 9d). This observation further supports the structure-reinforcing role of **GS** hydrogen bonding and explains the observation of different isotherms for the two monolayers.

The evolution of the structural changes during compression of the guanidinium-free C16BPS:C6BP monolayer is apparent from new Bragg peaks (q_{xy}) that emerge at various surface pressures (Figure 11). The data obtained upon compression to

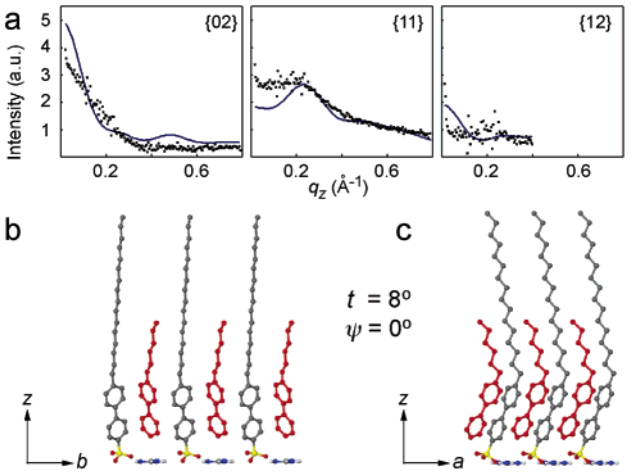

Figure 10. (a) Experimental (black dots) and calculated (blue lines) Bragg rod intensity profiles, $I(q_z)$, for (**G**)C16BPS:C6BP as refined with the rotated shifted ribbon (Figure 6b) hydrogen bonding motif. The refined packing arrangement of the (**G**)C16BPS:C6BP monolayers with the rotated shifted ribbon motif as viewed down the (c) *a* and (d) *b* axes. The C6BP guest molecules are depicted in red. The angles *t* and ψ are defined in Figure 6.

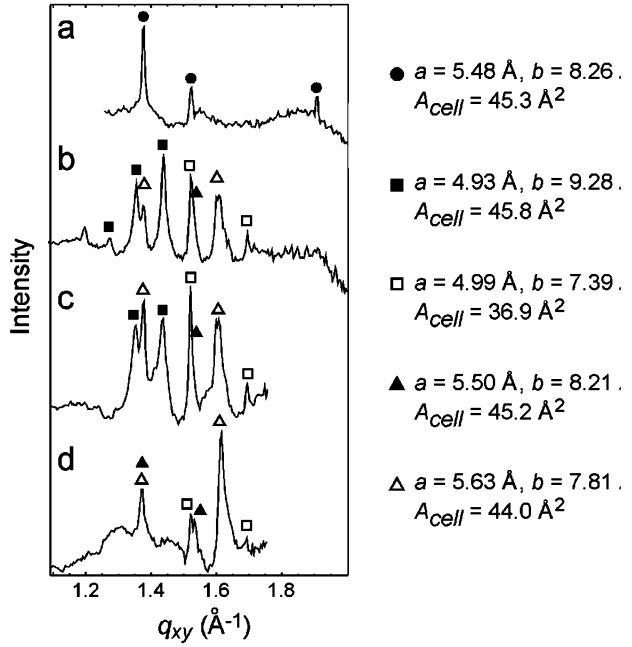

Figure 11. Bragg peaks of C16BPS:C6BP on pure water at (a) 40 < A_{mol} <60 Å^2/sulfonate, (b) A_{mol} = 30 Å^2/sulfonate, (c) A_{mol} = 30 Å^2/sulfonate, after 7 min, and (d) A_{mol} = 23 Å^2/sulfonate. The Bragg peaks are tentatively assigned to the following phases: (solid circle) parent C16BPS:C6BP monolayer; (solid square) an intermediate phase, possibly with two guests alligned vertically end-to-end between the amphiphiles; (open square) C16BPS monolayer; (solid triangle) C6BP multilayer; (open triangle) monolayer beneath C6BP multilayer. The unit cell dimensions of the C6BP multilayer are similar to those of bulk C6BP.

30 Å^2/sulfonate suggest multiple phases, including the guest-free C16BPS monolayer (Figure 3c) and two new phases with unit cell dimensions differing slightly from the original C16BPS:C6BP monolayer (each phase can be identified from the sets of Bragg peaks with fwhm values corresponding to an equal coherence length). The relative amounts of these phases, as deduced from the Bragg peak intensities, change with time while the surface pressure is held constant at 30 Å^2/sulfonate. As the monolayer is compressed further to <25 Å^2/sulfonate, the Bragg peaks associated with one of the new phases disappears.

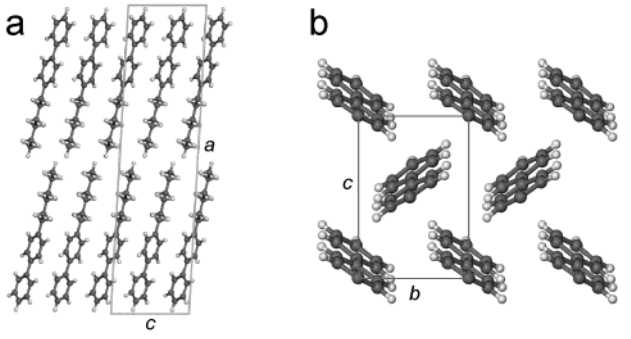

Figure 12. The herringbone layers of C6BP displayed in the 3-D single-crystal structure. The alkyl chains in (b) have been omitted for clarity.

Although the limited amount of data precluded definitive structural assignments of these transient phases, a plausible explanation for this behavior is the pressure-induced expulsion of the C6BP guests, initially producing C6BP inclusions at the top of the monolayer followed by a C6BP multilayer on top of the guest-free C16BPS monolayer. The presence of a multilayer is supported by narrow Bragg rods which exhibited a fwhm corresponding to a film thickness of 140 Å. The Bragg peaks at q_{xy} = 1.375 and 1.530 Å^{-1} associated with these rods were indexed to a rectangular unit cell with in-plane dimensions of 5.50 and 8.21 Å. Notably, C6BP single crystals grow from methanol as extremely thin plates. Single-crystal X-ray diffraction[32] at −173 °C revealed $P2_1/c$ symmetry (a = 31.558 Å, b = 5.377 Å, c = 7.943 Å, β = 93.216°) and (100) bilayers of C6BP molecules in a herringbone arrangement within each layer (Figure 12). Powder X-ray diffraction (PXRD) of bulk C6BP at 0 °C, near the 4 °C operating temperature of the GIXD, also revealed a monoclinic lattice but with slightly expanded lattice dimensions (a = 32.50 Å, b = 5.59 Å, c = 8.24 Å, β = 93.56°) compared with −173 °C owing to thermal expansion. The bulk b and c cell dimensions measured by PXRD at 0 °C are essentially identical with the in-plane lattice constants determined for the multilayer by GIXD. The GIXD Bragg peaks at q_{xy} = 1.530 Å^{-1} and q_{xy} = 1.375 Å^{-1} correspond to the (002) and (011) reflections of bulk C6BP, respectively. The (001) and (010) reflections, which have d spacings within the measured q_{xy} range, are not allowed by the $P2_1/c$ space-group symmetry. The agreement of the PXRD and GIXD lattice parameters and the proclivity of C6BP to organize as bilayers with a thin plate crystal morphology are consistent with the formation of a C6BP multilayer. Unfortunately, corroboration of this putative multilayer with atomic force microscopy (AFM) of LB films on mica substrates was precluded by the low melting point of C6BP (31 °C), near the operating temperature of the AFM.

Tetracosane Intercalate. To examine the importance of biphenyl−biphenyl host−guest interactions to monolayer structure and stability, tetracosane (C24), which has a length comparable with C16BP but lacks the biphenyl group, was examined as a guest molecule. The π−A isotherm of C16BPS:C24 spread over pure water was similar to the isotherm obtained over 0.01 M **G**2CO$_3$, with $A_{lift-off}$ = 50 Å^2/sulfonate, a transition to a second phase at 46 Å^2/sulfonate, and a plateau

(32) Single-crystal X-ray structure data for 4-hexylbiphenyl (**5**): formula $C_{18}H_{22}$; formula weight 238.36; crystal system monoclinic; space group $P2_1/c$; a = 31.558(2) Å; b = 5.377(5) Å; c = 7.943(5) Å; β = 93.216(2); V = 1345.8(2) Å^3, temperature 100(1) K; Z = 4; R1($I > 2\sigma(I)$) = 0.1527; wR2($I > 2\sigma(I)$) = 0.3604; GOF = 1.071.

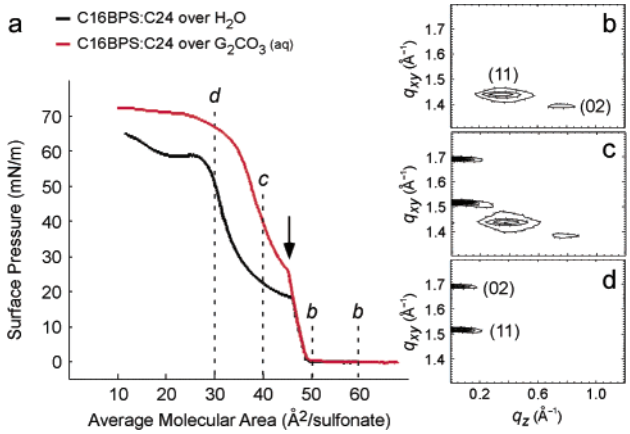

Figure 13. (a) $\pi-A$ isotherms of C16BPS:C24 on pure water (black) and on 0.01 M $\mathbf{G}_2CO_3$ (red). GIXD contour plots of the scattered intensity measured for C16BPS:C24 on pure water at (b) $50 < A_{mol} < 70$ Å^2/sulfonate, where the crystalline phase is characterized by tilted alkyl chains, (c) 40 Å^2/sulfonate, where two phases are evident, and (d) 32 Å^2/sulfonate, corresponding to a second phase with alkyl chains that are oriented normal to the air−water interface. The GIXD contour plots measured for C16BPS:C24 on 0.01 M aqueous $\mathbf{G}_2CO_3$ (not shown) are identical with the patterns above at corresponding positions on the isotherm.

at ca. 30 Å^2/sulfonate (Figure 13a). The transitions at 46 and ca. 30 Å^2/sulfonate occur at lower surface pressures over pure water compared with 0.01 M $\mathbf{G}_2CO_3$.

The GIXD patterns for C16BPS:C24 on pure water and 0.01 M $\mathbf{G}_2CO_3$ were identical. At $50 < A_{mol} < 70$ Å^2/sulfonate (Figure 13b), these data support the presence of a single crystalline phase ($a = 4.99$ Å, $b = 9.04$ Å, $\gamma = 90°$, $A_{cell} = 45.1$ Å^2) and alkyl chains tilted 29° from the normal along the *b* axis (herein referred to as phase I). The C16BPS:C24 packing arrangement was determined by refinement based on an asymmetric unit containing C16BPS and C24, each constrained as separate rigid bodies. Molecular models revealed that the shorter *a* axis and longer *b* axis of phase I, relative to the aforementioned inclusion monolayers, promote dense packing of the host and guest alkyl chains. The *a* and *b* lattice parameters of phase I, however, are inconsistent with any reasonable in-plane hydrogen bonding for a **GS** sheet like that observed in bulk crystals and the aforementioned monolayers. The refined structure was consistent with all-trans C24 and C16 alkyl chains organized in a pseudo-herringbone arrangement (Figure 14c,d), with the C24 chains elevated above the biphenyl groups and protruding from the upper surface of the C16BPS layer. Notably, the structural refinement indicated that the GIXD data could be attributed solely to scattering from close-packed C24 and C16 alkane chains, i.e., by ignoring scattering contributions from the biphenyl and sulfonate moieties of the C16BPS amphiphiles. This is consistent with disorder of the biphenylsulfonate moiety of the amphiphile due to loose packing of the biphenyl groups and the absence of an ordered **GS** network.

The diffraction pattern collected at $A_{mol} = 40$ Å^2/sulfonate (Figure 13c), i.e., at a molecular area below the phase transition, revealed the emergence of a second crystalline phase (herein referred to as phase II) that coexists with phase I but has a smaller unit cell ($a = 4.99$ Å, $b = 7.43$ Å, $\gamma = 90°$, $A_{cell} = 37.1$ Å^2) and alkyl chains perpendicular to the air−water interface. Further compression to 32 Å^2/sulfonate afforded a GIXD pattern attributable to only phase II (Figure 13d). The coherence lengths for the low- and high-pressure phases are 200 and 700 Å, respectively. The refined structure for phase II is consistent with packing of all-trans alkyl chains organized in a parallel arrangement (Figure 14e,f). Like phase I, the scattering intensity could be attributed solely to the close-packed alkyl chains.

It also is reasonable to suggest that at higher surface pressures the alkane guest can be expelled from the C16BPS monolayer. The Bragg peaks for phase II at $q_{xy} = 1.52$ and 1.69 Å^{-1} at $A_{mol} < 32$ Å^2/sulfonate are identical in position with those produced by both a C16BPS monolayer alone (Figure 3) and also with those reported for a crystalline C24 bilayer[33] in the presence of 10 mol % $C_{28}H_{57}OH$. The scattering pattern produced by a heterobilayer composed of C24 overlayer on an underlying C16BPS monolayer at the air−water interface thus would consist of a combination of coinciding Bragg peaks corresponding to the identical unit cell dimensions of the two individual crystalline layers. The intensities of the Bragg peaks for phase II are substantially larger (ca. 50× at $A_{mol} = 32$ Å^2/sulfonate) than those observed for the C16BPS monolayer alone (Figure 15), indicating that phase II is more crystalline. Tapping mode AFM of LB films of phase II, transferred to a mica substrate at 50 mN/m, revealed the presence of a 28 Å thick film. This is consistent with the existence of a mixed monolayer rather than a heterobilayer, which would be expected to exhibit a thickness of 60 Å. The 28 Å thickness is consistent with that expected for a C16BPS monolayer with vertically aligned chains. This is not unexpected, as the segments of the C24 molecules that protrude from the upper surface of the C16BPS monolayer are most likely disordered such that the AFM tip penetrates to the surface where the C16 and C24 alkyl chains become close-packed.

These observations combined argue that the structure of this mixed monolayer, for which the biphenyl group is absent in the nonamphiphilic intercalate, is governed by alkane−alkane interactions to produce a packing motif that is incompatible with formation of the **GS** network. The absence of an ordered **GS** sheet and the pressure-induced expulsion of the alkane guest molecules illustrate that biphenyl−biphenyl interactions play an important role in the formation and stabilization of inclusion monolayers based on this host. This suggests that the achievement of a stable ternary inclusion monolayer relies on guests that are homologous with the hydrophobe of the organosulfonate amphiphile. The importance of the biphenyl−biphenyl interactions are corroborated by GIXD measurements on monolayers containing *p*-chlorohexadecylbiphenyl guest within the (**G**)-C16BPS host, for which GIXD data revealed that the chloro substituent excluded **G** from the air−water interface, apparently to preserve the biphenyl−biphenyl interactions (see the Supporting Information).

Summary

Crystalline ternary inclusion monolayers consisting of a two-dimensional hydrogen-bonded host network of guanidinium (**G**) ions and organosulfonate (**S**) amphiphiles, and biphenylalkane guests, can be generated at the air−water interface through synergistic structural enforcement by hydrogen bonding and host−guest packing. The structure of these monolayer inclusion compounds resembles the interdigitated bilayer structures of

(33) Weinbach, S. P.; Weissbuch, I.; Kjaer, K.; Bouwman, W. G.; Nielsen, J. A.; Lahav, M.; Leiserowitz, L. *Adv. Mater.* **1995**, *7*, 857.

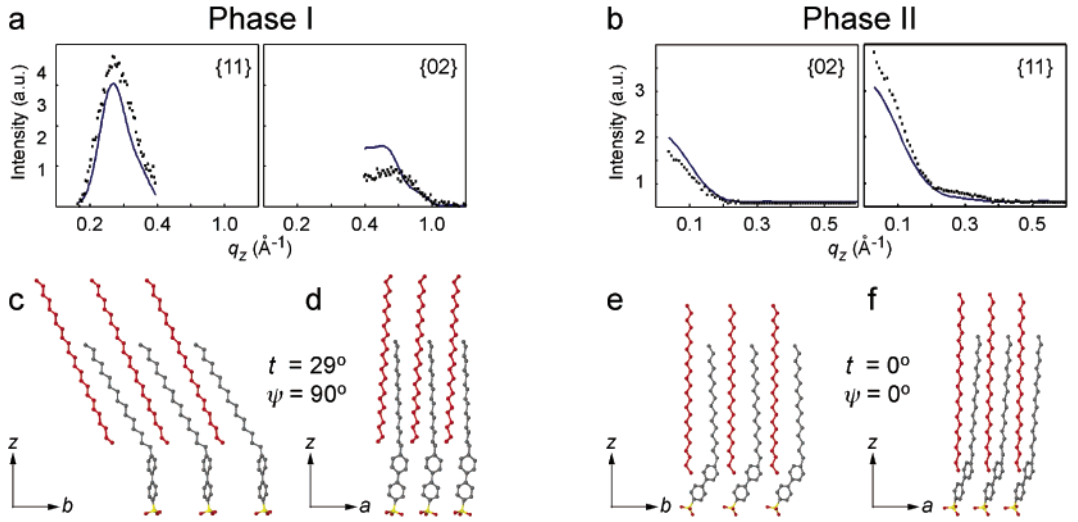

Figure 14. Experimental (black dots) and calculated (blue lines) Bragg rod intensity profiles, $I(q_z)$, for as refined for (a) phase I C16BPS:C24 at $50 < A_{mol} < 70$ Å^2/sulfonate and (b) phase II C16BPS:C24 at $A_{mol} < 32$ Å^2/sulfonate. The refined packing arrangement of the phase I and phase II as viewed down the (c, e) *a* and (d, f) *b* axes, respectively. The C24 molecules are depicted in red. The angles *t* and ψ are defined in Figure 6.

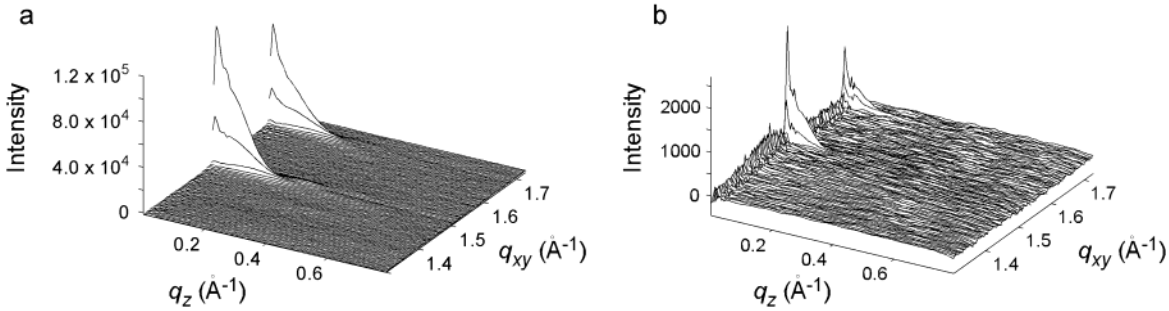

Figure 15. GIXD surface plots of the scattered intensity measured for (a) the C16BPS:C24 monolayer on pure water and compressed to 40 Å^2/sulfonate and (b) C16BPS on pure water over all areas measured. These GIXD patterns display identical peak positions at $q_{xy} = 1.52$ and 1.70 Å^{-1}, but the intensity in (a) is ca. 50 times greater than that in (b).

(**G**)C1BPS and (**G**)C2BPS (Figure 2), with the nonamphiphilic guests supplanting the organosulfonate residues of the opposing **GS** sheet. Interestingly, attempts to crystallize bulk inclusion compounds based on (**G**)C6BPS and (**G**)C10BPS with their isomorphous guests were not successful, as only guest-free compounds[34] with a continuously interdigitated layer architecture[35] were obtained. This indicates that the topology of the monolayer inclusion compounds, in which all the organosulfonate residues project from the upper side of the **GS** sheet, is unique to the air−water interface. The ability to sustain ternary host−guest phases with the **GS** network intact appears to require guests that are structurally homologous, in the strictest sense, with the organosulfonate substituents. It is important to note that the absence of GIXD peaks due to separate monolayer phases or multilayers of biphenylalkane guests with $n > 6$ proves that these guest molecules are included within the host monolayer in a 1:1 stoichiometry, as expected from the composition of the spreading solution. The observation of these monolayer inclusion compounds suggests an approach for the design and synthesis of functional monolayers in which nonamphiphilic molecules adorned with desired functionality can be anchored at the air−water interface through intercalation in host inclusion cavities with well-defined metrics. Such an approach offers the prospect of separating the function of the monolayer (i.e., the guest) from the inherent structure of the host, avoiding the requirement of designing functional molecules that are also amphiphilic.

Experimental Section

Materials Synthesis and General Procedures. 4-Chlorobiphenyl was purchased from TCI America and used as received. Tetrahydrofuran (Aldrich) was distilled under argon over potassium and benzophenone prior to use. All other solvents and starting materials were purchased as ACS grade from Aldrich and were used directly as received. Guandinium tetrafluoroborate, which was used for the synthesis of guanidinium biphenylalkanesulfonate salts, was synthesized by combining equimolar amounts of guanidinium carbonate and tetrafluroboric acid in acetone, followed by filtration to yield (**G**)BF_4 as the precipitate. All reactions were performed under a nitrogen or argon atmosphere. ^{1}H NMR spectra were recorded on a Varian Inova 500 spectrometer. Mass spectrometry (MS) was performed with a high-resolution Finnigan MAT 95 instrument. Grazing angle infrared spectra of Langmuir−Blodgett films were recorded with a Nicolet Magna 550 FT-IR equipped with a Harrick Seagull reflectance accessory and an MCT detector, at an incident angle of 86° with unpolarized light and 4 cm^{-1} spectral resolution. The LB films for FT-IR studies were prepared by transfer

(34) Single-crystal X-ray structure data for (**G**)(4′-hexylbiphenyl-4-sulfonate): formula $C_{19}H_{27}N_3O_3S$; formula weight 377.51; crystal system orthorhombic; space group $P2_12_12_1$; $a = 7.4862(11)$ Å; $b = 7.6555(12)$ Å; $c = 33.449(5)$ Å; $V = 1917.0(5)$ Å^3, temperature 173(2) K; $Z = 4$; R1($I > 2\sigma(I)$) = 0.0420; wR2($I > 2\sigma(I)$) = 0.1112; GOF = 1.105. Single-crystal X-ray structure data for (**G**)(4′-decylbiphenyl-4-sulfonate): formula $C_{23}H_{35}N_3O_3S$; formula weight 433.61; crystal system monoclinic; space group $P2_1/c$; $a = 7.668(9)$ Å; $b = 7.923(8)$ Å; $c = 38.321(3)$ Å; $\beta = 92.89(3)$; $V = 2325.7(0)$ Å^3, temperature 173(2) K; $Z = 4$; R1($I > 2\sigma(I)$) = 0.1110; wR2($I > 2\sigma(I)$) = 0.2138; GOF = 1.095.

(35) Horner, M. J.; Holman, K. T.; Ward, M. D. *Angew. Chem., Int. Ed.* **2001**, *40*, 4045.

of Langmuir monolayers to gold-coated glass microscope slides. Atomic force microscopy (AFM) was performed in tapping mode with a Nanoscope IIIa Multimode system (Digital Instruments, Santa Barbara, CA), a scanner with a maximum 15 μm scan range, and a 90 μm Si cantilever tip (MikroMasch, Tallinn, Estonia) with an Al-coated backside, force constant of 14 N/m, and resonant frequency of 270 kHz. All data were acquired in height mode with a scan rate of 2 Hz. The LB films for AFM measurements were prepared by transfer of the Langmuir monolayers to a mica substrate (Ted Pella Inc.). Only of the mica substrate was coated, so that the film thickness could be measured relative to the bare mica surface.

4-*n*-Hexadecylbiphenyl (C16BP). Hexadecylmagnesium bromide, prepared from 5.18 g (0.22 mol) of magnesium turnings and 40 mL (0.13 mol) of *n*-hexadecyl bromide in 250 mL of tetrahydrofuran, was added dropwise via cannula to a stirred tetrahydrofuran solution of 27.16 g (0.13 mol) of 4-chlorobiphenyl and 138 mg (0.26 mmol) of $NiCl_2$-(dppe) in 500 mL of tetrahydrofuran at 4 °C. The hexadecylmagnesium bromide solution was transferred hot in order to prevent precipitation in the cannula. The resulting yellow-green reaction mixture was stirred for 2 h at 4 °C, warmed to room temperature over 3 h, and heated at reflux overnight. The reaction mixture was quenched in 500 mL of water, acidified to pH 1 with concentrated aqueous HCl (12 M), and extracted twice with 200 mL of methylene chloride. The combined organic layers were dried over magnesium sulfate and filtered, and the solvent was removed under reduced pressure. The resulting orange solid was passed through a plug of silica gel to remove the colored impurities associated with the $NiCl_2$(dppe) catalyst. The product, which is a solid at room temperature but melts at 66 °C, was isolated from the reaction mixture by fractional distillation to yield a white powder that was sufficiently pure and did not require recrystallization (total yield 22 g, 45%): mp 66 °C, bp 220/4 mmHg. ^{1}H NMR (CD_2Cl_2, 500 MHz): δ 7.61 ppm (d, 2H, Ar H), 7.53 (d, 2H, Ar H), 7.44 (t, 2H, Ar H), 7.34 (t, 1H, Ar H), 7.28 (d, 2H, Ar H), 2.66 (t, 2H, CH_2-1′), 1.65 (m, 2H, CH_2-2′), 1.28 (m, 26H, CH_2), 0.90 (t, 3H, CH_3). MS: *m*/*z* 378.32. Anal. Calcd for $C_{28}H_{42}$: C, 88.82; H, 11.18. Found: C, 88.77; H, 11.04.

4-*n*-Decylbiphenyl (C10BP). Using a procedure analogous to that for C16BP, 5 mL of *n*-decyl bromide was converted into 4-*n*-decylbiphenyl. The product was purified by fractional distillation and recrystallized from hexane to obtain a white powder: total yield 3.9 g, 55%; mp 55 °C, bp 210 °C/2 mmHg. ^{1}H NMR (CD_2Cl_2, 500 MHz): δ 7.61 ppm (d, 2H, Ar H), 7.53 (d, 2H, Ar H), 7.44 (t, 2H, Ar H), 7.34 (t, 1H, Ar H), 7.28 (d, 2H, Ar H), 2.66 (t, 2H, CH_2-1′), 1.64 (m, 2H, CH_2-2′), 1.29 (m, 14H, CH_2), 0.90 (t, 3H, CH_3). Anal. Calcd for $C_{22}H_{30}$: C, 89.73; H, 10.27. Found: C, 88.57; H, 10.28.

4-*n*-Hexylbiphenyl (C6BP). Using a procedure analogous to that for C16BP, 8.2 mL of *n*-hexyl bromide was converted into 4-*n*-hexylbiphenyl. The product was purified by fractional distillation and recrystallized from methanol to obtain extremely thin plates with crystal dimensions 0.06 mm × 0.03 mm × 0.002 mm: total yield 5 g, 40%; mp 31 °C, bp 150 °C/3 mmHg. ^{1}H NMR (CD_2Cl_2, 500 MHz): δ 7.63 ppm (d, 2H, Ar H), 7.56 (d, 2H, Ar H), 7.46 (t, 2H, Ar H), 7.36 (t, 1H, Ar H), 7.30 (d, 2H, Ar H), 2.68 (t, 2H, CH_2-1′), 1.68 (m, 2H, CH_2-2′), 1.37 (m, 6H, CH_2), 0.94 (t, 3H, CH_3). Anal. Calcd for $C_{18}H_{22}$: C, 90.70; H, 9.30. Found: C, 90.79; H, 9.22.

4-*n*-Butylbiphenyl (C4BP). Using a procedure analogous to that for C16BP, 6.26 mL of *n*-butyl bromide was converted into 4-*n*-butylbiphenyl. The product was purified by fractional distillation to obtain a clear liquid: total yield 4 g, 33%; bp 140 °C/3 mmHg. ^{1}H NMR (CD_2Cl_2, 500 MHz): δ 7.62 ppm (d, 2H, Ar H), 7.54 (d, 2H, Ar H), 7.45 (t, 2H, Ar H), 7.35 (t, 1H, Ar H), 7.29 (d, 2H, Ar H), 2.68 (t, 2H, CH_2-1′), 1.66 (m, 2H, CH_2-2′), 1.41 (m, 2H, CH_2), 0.98 (t, 3H, CH_3).

1-Bromo-4-hexadecylbenzene. A hot solution of *n*-hexadecylmagnesium bromide, prepared from 0.84 g of magnesium turnings and 7.13 mL (23.1 mmol) of *n*-bromohexadecane in 25 mL of tetrahydrofuran, was added dropwise via cannula to a stirred solution of 5 g (21 mmol) of *p*-dibromobenzene and 0.17 g of $NiCl_2$(dppf) (0.21 mmol) in 25 mL of tetrahydrofuran at 4 °C. The resulting reaction mixture was stirred for 1 h at 4 °C, warmed to room temperature, and heated at reflux overnight. The reaction mixture was quenched in 50 mL of water, acidified with an aqueous HCl solution to pH 1, and extracted twice with 20 mL of methylene chloride. The combined organic layers were dried over magnesium sulfate and filtered, and the solvent was removed under reduced pressure. The product was purified from by flash chromatography with hexane to yield the product as a white powder after removal of the hexane solvent: total yield 6.9 g, 96%. ^{1}H NMR (CD_2Cl_2, 500 MHz): δ 7.40 ppm (d, 2H, Ar H), 7.08 (d, 2H, Ar H), 2.57 (t, 2H, CH_2-1′), 1.58 (m, 2H, CH_2-2′), 1.27 (m, 26H, CH_2), 0.89 (t, 3H, CH_3).

4′-Chloro-4-*n*-hexadecylbiphenyl (C16BP-Cl). Using a procedure identical with that for 1-bromo-4-hexadecylbenzene, C16BP-Cl was prepared by the addition of 1-(magnesium bromide)-4-hexadecylbenzene to an equimolar amount of 1-bromo-4-chlorobenzene in tetrahydrofuran. The product was purified by flash chromatography with hexane to yield the product as a white powder after removal of the hexane solvent: total yield 0.95 g, 77%; mp 75 °C. ^{1}H NMR (CD_2Cl_2, 500 MHz): δ 7.56 ppm (d, 2H, Ar H), 7.50 (d, 2H, Ar H), 7.42 (d, 2H, Ar H), 7.28 (d, 2H, Ar H), 2.66 (t, 2H, CH_2-1′), 1.65 (m, 2H, CH_2-2′), 1.28 (m, 26H, CH_2), 0.90 (t, 3H, CH_3). MS: *m*/*z* 412.29. Anal. Calcd for $C_{28}H_{41}Cl$: C, 81.41; H, 10.01; Cl, 8.58. Found: C, 81.71; H, 9.86; Cl, 8.63.

4′-*n*-Hexadecylbiphenyl-4-sulfonic acid (C16BPS). Chlorosulfonic acid 0.97 mL (14.5 mmol) was added dropwise to a stirred solution of 5 g (13 mmol) of 4-*n*-hexadecylbiphenyl in 125 mL of chloroform. The mixture was stirred under nitrogen for 5 h, after which the solvent was removed under reduced pressure. The product was obtained as a white powder upon recrystallization from acetonitrile: total yield 6 g, 90%. ^{1}H NMR (DMSO, 500 MHz): δ 7.63 (d, 2H, Ar H), 7.57 (d, 2H, Ar H), 7.56 (d, 2H, Ar H), 7.26 (d, 2H, Ar H), 2.59 (t, 2H, CH_2-1′), 1.5 (m, 2H, CH_2-2′), 1.22 (m, 26H), 0.84 (t, 3H, CH_3). Anal. Calcd for $C_{28}H_{42}O_3S$: C, 71.32; H, 9.23; S, 6.99. Found: C, 71.13; H, 9.50; S, 6.52.

Guanidinium 4′-Decylbiphenyl-4-sulfonate ((G)C10BPS). Using a procedure similar to that employed for C16BPS, 4′-*n*-decylbiphenyl-4-sulfonic acid was prepared from 4-decylbiphenyl. The guanidinium salt was prepared by treatment of the sulfonic acid with a saturated acetone solution of guanidinium tetrafluoroborate (roughly a 5-fold molar excess of guanidinium), which afforded the product as a white precipitate that was isolated by filtration and recrystallized from methanol as colorless needles: mp 177 °C. ^{1}H NMR (DMSO, 500 MHz): δ 7.68 (d, 2H, Ar H), 7.62 (d, 2H, Ar H), 7.61 (d, 2H, Ar H), 7.31 (d, 2H, Ar H), 6.95 (s, 6H, $(NH_2)_3$), 2.63 (m, 2H, CH_2), 1.61 (m, 2H, CH_2), 1.27 (m, 14H, CH_2), 0.82 (t, 3H, CH_3).

Guanidinium 4′-Hexylbiphenyl-4-sulfonate ((G)C6BPS). Using a procedure similar to that employed for C16BPS, 4′-*n*-hexylbiphenyl-4-sulfonic acid was prepared from 4-hexylbiphenyl. The guanidinium salt was prepared by treatment of the sulfonic acid with a saturated acetone solution of guanidinium tetrafluoroborate (roughly a 5-fold molar excess of guanidinium), which afforded the product as a white precipitate that was isolated by filtration and recrystallized from methanol as colorless needles: mp 244 °C. ^{1}H NMR (DMSO, 500 MHz): δ 7.64 (d, 2H, Ar H), 7.58 (d, 2H, Ar H), 7.56 (d, 2H, Ar H), 7.26 (d, 2H, Ar H), 6.91 (s, 6H, $(NH_2)_3$), 2.59 (m, 2H, CH_2), 1.57 (m, 2H, CH_2), 0.85 (t, 3H, CH_3).

Guanidinium 4′-Ethylbiphenyl-4-sulfonate ((G)C2BPS). Using a procedure similar to that employed for C16BPS, 4′-*n*-ethylbiphenyl-4-sulfonic acid was prepared from 4-ethylbiphenyl. The guanidinium salt was prepared by treatment of the sulfonic acid with a saturated acetone solution of guanidinium tetrafluoroborate (roughly a 5-fold molar excess of guanidinium), which afforded the product as a white precipitate that was isolated by filtration and recrystallized from methanol as colorless needles: mp 296 °C. ^{1}H NMR (DMSO, 500

MHz): δ 7.63 (d, 2H, Ar H), 7.57 (d, 2H, Ar H), 7.56 (d, 2H, Ar H), 7.28 (d, 2H, Ar H), 6.90 (s, 6H, $(NH_2)_3$), 2.62 (q, 2H, CH_2), 1.86 (t, 3H, CH_3).

Guanidinium 4′-Methylbiphenyl-4-sulfonate ((G)C1BPS). Using a procedure similar to that employed for C16BPS, 4′-*n*-methylbiphenyl-4-sulfonic acid was prepared from 4-methylbiphenyl. The guanidinium salt was prepared by treatment of the sulfonic acid with a saturated acetone solution of guanidinium tetrafluoroborate (roughly a 5-fold molar excess of guanidinium), which afforded the product as a white precipitate that was isolated by filtration and recrystallized from methanol as colorless needles: mp 294 °C. ^{1}H NMR (DMSO, 500 MHz): δ 7.65 (d, 2H, Ar H), 7.59 (d, 2H, Ar H), 7.55 (d, 2H, Ar H), 7.26 (d, 2H, Ar H), 6.94 (s, 6H, $(NH_2)_3$), 2.33 (t, 3H, CH_3).

Surface Pressure−Area (π−*A*) Isotherms and Langmuir Blodgett (LB) Films. Langmuir isotherms were recorded on a Nima Langmuir trough (Model No. 611) (trough area 10 cm × 30 cm) at a compression rate of 5 mm/min and a subphase temperature of 20.0 ± 0.1 °C. The aqueous subphase was prepared with deionized water (purified to 17.9 MΩ cm with a Barnstead water purifier) and the selected solute, if any. Surface pressure was recorded with a Wilhelmy balance and a paper plate. All monolayers were prepared by the introduction of chloroform solutions containing 1% methanol (v/v), C16BPS (0.4−0.8 mg/mL), and an equimolar amount of CnBP, C16BP-Cl, or C24 (if any). Before isotherms were collected, monolayers formed from mixed spreading solutions were annealed by compressing the barriers until a surface pressure of 1 mN/m was achieved and then expanding the barriers to their initial position.

Grazing Incidence X-ray Diffraction. GIXD for the monolayers was performed using the liquid surface diffractometer on the undulator beam line BW1 in HASYLAB at DESY (Hamburg, Germany).[36] A sealed and temperature-controlled Langmuir trough (4 °C), equipped with a Wilhelmy balance for surface pressure measurement of the films, was mounted on the diffractometer. Monochromatic synchrotron radiation ($\lambda = 1.3037$ Å) was produced by Bragg reflection from a Be crystal. Surface sensitivity was optimized by adjustment of the incident grazing angle of the beam, with respect to the monolayer surface, to $\alpha_i = 0.85\alpha_c$ (where $\alpha_c = 0.138°$, the critical angle for total external reflection), which creates an evanescent wave with a minimal penetration depth and reduces scattering due to the subphase. The footprint of the incident X-ray beam at the air−water interface was 5 mm × 50 mm, and the diffracted radiation was recorded with a one-dimensional position-sensitive detector (PSD), which resolved the vertical component of the X-ray scattering vector, $q_z \cong (2\pi/\lambda) \sin \alpha_f$ (where α_f is the angle between the diffracted beam and the horizon), over the range $0.0 \le q_z \le 1.4$ Å^{-1}. The PSD was mounted vertically behind a horizontally collimating Soller slit with a horizontal resolution width $\Delta(q_{xy}) = 0.007$ Å^{-1}. The GIXD patterns were measured by scanning over a range of the horizontal component of the X-ray scattering vector, $q_{xy} \cong (4\pi/\lambda) \sin \theta_{xy}$, where $2\theta_{xy}$ is the horizontal scattering angle between the beam and the Soller collimator. The GIXD diffraction data can be presented in three ways: (1) as a two-dimensional intensity distribution $I(q_{xy},q_z)$ in a surface or contour plot, (2) as Bragg peaks $I(q_{xy})$ obtained by measuring the scattered intensity over the range of q_{xy} and integrating over the entire q_z range of the PSD, and (3) as Bragg rod intensity profiles $I(q_z)$ obtained from the scattered intensity recorded in channels along the PSD and integrated over the q_{xy} range corresponding to a specific Bragg peak.

Molecular models of 2-D crystalline monolayers were constructed using the CERIUS^2 or Molecular Studio computational packages[37] and previously determined bulk crystal structures as a guide. Least-squares structural refinements based on these models and the GIXD data were performed using SHELX-97.[38] Although this software package is designed for bulk single crystals, refinement of a 2-D structure can be achieved with the following procedure.[39,40] The continuous Bragg rod intensities distributed along q_z, $|F^2(h,k,q_z)|^2$, were transformed into discrete reflection data sets, $|F(h,k,l)|^2$, wherein a particular Miller index l is associated with a virtual c axis calculated as $c = 2\pi/\Delta q$, where q_z is sampled in steps of $-\Delta q_z$. The superposition of the $|F(h,k,q_z)|^2$ and $|F(-h,-k,q_z)|^2$ Bragg rods, a property of the measured GIXD powder pattern, was simulated in SHELX-97 by imposing a twinning of the crystal about the *ab* plane. Because of the limited amount of diffraction data, refinement could only be performed with the molecular constituents constrained as rigid bodies, fixed within the measured unit cell dimensions. Following the refinement, the calculated structure factor $|F^2(h,k,l)|$ was converted to the calculated Bragg rod intensity profile $|F(h,k,q_z)|^2$, which was then compared with the experimental data. This comparison allows direct visual inference of the quality of the refined structure.

Single-Crystal X-ray Structural Analysis. Experimental parameters pertaining to the single-crystal X-ray analyses of the various guanidinium 4′-alkylbiphenyl-4-sulfonates are provided in the references. CIF files are included as Supporting Information. Data were collected at the X-ray Crystallographic Laboratory in the Department of Chemistry at the University of Minnesota with a Bruker CCD platform diffractometer with graphite-monochromated Mo Kα radiation (λ = 0.710 73 Å) at 173(2) K. The structures were solved by direct methods and refined with full-matrix least-squares/difference Fourier analysis using the SHELX-97 suite of software. All non-hydrogen atoms were refined with anisotropic displacement parameters, and all hydrogen atoms were placed in idealized positions and refined with a riding model. Data were corrected for the effects of adsorption using SADABS. Single-crystal structural analysis of 4-hexylbiphenyl crystals, grown from methanol as very thin plates (0.06 × 0.03 × 0.002 mm; see above), was performed by Dr. Victor Young using the APS synchrotron at sector 15-C with a frame time of 3 s and a detector distance of 4.9 cm with the Bruker Kappa/SMART 6000 microdiffractometer and $\lambda = 0.5594$ Å at 100(1) K. A randomly oriented region of reciprocal space was surveyed to the extent of 2.0 hemispheres and to a resolution of 0.84 Å with ψ scans. The intensity data were corrected for absorption and decay (SADABS[41]). Final cell constants were calculated from 3155 reflections from the actual data collection after integration (SAINT[42]). The structure was solved using SIR-97.[43] A direct-methods solution was calculated, which provided most non-hydrogen atoms from the *E* map. Full-matrix least-squares/difference Fourier cycles were performed, which located the remaining non-hydrogen atoms. All non-hydrogen atoms were refined with isotropic displacement parameters. All hydrogen atoms were placed in ideal positions and refined as riding atoms with relative isotropic displacement parameters.

Acknowledgment. This work was supported by the IHP-Contract HPRI-CT-1999-00040/2001-00140 of the European Commission, the United States−Israel Binational Science Foundation (BSF), the Danish Foundation for Natural Science, and the National Science Foundation (DMR-0305278). We thank HASYLAB, DESY, Hamburg, Germany, for beam time

(36) Jensen, T. R.; Kjaer, K. Structural Properties and Interactions of Thin Films at the Air−Liquid Interface Explored by Synchrotron X-ray Scattering. In *Novel Methods to Study Interfacial Layers*; Moebius, D., Miller, R., Eds.; Studies in Interface Science 11; Elsevier Science: Amsterdam, 2001; pp 205−254.
(37) CERIUS^2 (IRIX platform) and Materials Studio (Windows platform) computational packages, Accelrys, San Diego, CA.
(38) Sheldrick, G. M. SHELX-97 Program for Crystal Struture Determination; University of Göttingen, Göttingen, Germany, 1997.
(39) Weissbuch, I.; Baxter, P. N. W.; Kuzmenko, I.; Cohen, H.; Cohen, S.; Kjaer, K.; Howes, P. B.; Als-Nielsen, J.; Lehn, J. M.; Leiserowitz, L.; Lahav, M. *Chem. Eur. J.* **2000**, *6*, 725.
(40) Rapaport, H. Kuzmenko, I.; Lafont, S. Kjaer, K.; Howes, P. B.; Als-Nielsen, J.; Lahav, M.; Leiserowitz, L. *Biophys. J.* **2001**, *81*, 2729.
(41) Blessing, R. *Acta Crystallogr.* **1995**, *A51*, 33.
(42) SAINT V6.1, Bruker Analytical X-Ray Systems, Madison, WI.
(43) SIR-97: Altomare, A.; Burla, M. C.; Camalli, M.; Cascarano, G.; Giacovazzo, C.; Guagliardi, A.; Moliterni, A. G. G.; Polidori, G.; Spagna, R. (1997).

for GIXD experiments, Victor G. Young, Jr., and the X-ray Crystallographic Laboratory in the Department of Chemistry at the University of Minnesota for assistance with single-crystal X-ray structural analysis, and ChemMatCARS at Argonne National Laboratory for beam time made available for the collection of the C6BP crystal data. ChemMatCARS Sector 15 is supported principally by the National Science Foundation/ Department of Energy under Grant No. CHE0087817 and by the Illinois Board of Higher Education. The Advanced Photon Source is supported by the U.S. Department of Energy, Basic Energy Sciences, Office of Science, under Contract No. W-31-109-Eng-38.

Supporting Information Available: Complete GIXD data for all crystalline Langmuir monolayers, summary of GIXD data for (**G**)C16BPS:*p*-chlorohexadecylbiphenyl, measured and calculated X-ray powder diffraction data for C6BP, unit cell index and refinement report for C6BP, GIXD analysis for C16BPS:C16BP−Cl on water, atomic force microscopy data for the C16BPS:C24 LB film (Phase II), and single-crystal X-ray diffraction data (CIF format) for all reported bulk crystals. This material is available free of charge via the Internet at http://pubs.acs.org.

JA0371404